MODELING AND CONTROL OF A DOUBLY-FED INDUCTION GENERATOR IN A WIND TURBINE

García Verde, L. F.; Nájera Canal, S.; Rico Azagra, J.; Gil-Martínez, M.

Universidad de La Rioja

Nowadays, technology for management of wind energy is developing rapidly. Over the last few years variable speed wind turbines have overwhelmed their respective fixed-speed, mainly due to the improved performance they offer. The variable speed doubly-fed induction generator (DFIG) is one of the most frequently used in modern grid connected wind turbines, because it has the ability to fulfill the grid requirements. DFIG allows a precise control of frequency range, voltage and power generated.

For this purpose, this paper will focus on the analysis, modeling and control of the operation of a DFIG moved by a wind turbine and connected to the electricity grid. A nonlinear mathematical model of DFIG and its equivalent simplified model are described for simulation. It is also designed a rotor vector control and a control for the energy fed to the grid. A 2MW wind turbine is analyzed and simulated through Matlab/Simulink. Different reference frames will be used during the modeling and a suitable power control method over the machine operation will be introduced. Furthermore, it stresses the importance of vector control based on stator flux oriented technique in order to manage the active and reactive power effectively.

Keywords: DFIG; Vector control; Power control; Pitch control

MODELADO Y CONTROL DE GENERADOR DE INDUCCIÓN DOBLEMENTE ALIMENTADO DE UNA TURBINA EÓLICA

Hoy en día, la tecnología para la gestión de la energía eólica está avanzando rápidamente. Actualmente, las turbinas eólicas de velocidad variable han superado a las de velocidad fija, debido su mejor rendimiento. El generador de inducción doblemente alimentado (DFIG) se suele utilizar en turbinas eólicas conectadas a la red, ya que permite cumplir los requerimientos de calidad de red mediante un control preciso de la frecuencia, tensión y potencia generadas.

Con este fin, este artículo se centra en el análisis, modelado y control de un DFIG movido por una turbina eólica y conectado a la red eléctrica. Se describe el modelo matemático no lineal de simulación del DFIG y su modelo simplificado equivalente. También se diseña el control vectorial del rotor y el control de la energía inyectada a la red. Se analiza y simula el control de una turbina de viento de 2MW mediante Matlab/Simulink. Se utilizan diferentes sistemas de referencia y se introduce un control de potencia adecuado al funcionamiento de la máquina. Además, se hace hincapié en la importancia del control vectorial basado en la técnica de orientación de flujo del estator, con el fin de gestionar la potencia activa y reactiva con eficacia.

Palabras clave: DFIG; Control vectorial; Control de potencia; Control del ángulo de pala

Correspondencia: silvano.najerac@unirioja.es

1. Introduction

The interest for alternative energy sources has grown in recent years as a consequence of limited conventional resources and the exponential rise of environment pollution. In this sense, wind energy is becoming one of the most promising and economically affordable power sources.

One of the goals in the wind energy generation is to increase the efficiency of the energy transformation. In this direction, variable speed wind turbines have many advantages compared to fixed speed turbines. The integration of variable speed generators increase the power production at different wind speeds, extracting the maximum power as possible at low wind speeds while for strong winds, by controlling the pitch angle, the aerodynamic torque of the wind is limited preventing input mechanical power to exceed the design limits (Vázquez, González, Garrido, & Morilla, 2012).

The asynchronous electrical machine is the most popular type of generator because of its simplicity and robustness and also because of its low cost due to massive production. Its main drawback is the necessity for reactive current. The Doubly-Fed Induction Generator (DFIG) is becoming more and more widespread due to its ability to maximize the output power for the wind.

The DFIG is a wound rotor induction generator which has the rotor windings connected to a bidirectional back-to-back power converter. This type of generator has a larger range of variable speed operation. Another advantage of the DFIG is that the reactive power can be independently controlled by the rotor currents (Khemiri, Khedher, & Mimouni, 2012).

2. Wind model and pitch control

The power available in the wind passing through a circular area is:

$$P_m = \frac{1}{2} \cdot \rho \cdot A \cdot v^3 \quad [W] \tag{1}$$

where ρ is the density of dry air in [kg/m^3], v is the wind speed measured in [m/s] and A is the area swept by the blades [m^2].

A wind turbine can only extract part of this power, which is limited by the Betz limit. Only 16/27 or less of the kinetic energy in the wind can be converted to mechanical energy. Due to Betz' law, a power coefficient $C_p(\lambda, \beta)$ is defined, which is a function of the tip speed ratio λ and the attack or pitch angle of the rotor blades β. Thus, equation (1) becomes (Bujac, Stasiusk, & Valderrey, 2008; Varela & Valderrey, 2009):

$$P_m = \frac{1}{2} \cdot \rho \cdot A \cdot C_p(\lambda, \beta) \cdot v^3 \quad [W] \tag{2}$$

The tip speed ratio is defined as the relation between the rotational speed of the tip of the blade and the velocity of the wind as follows:

$$\lambda = \frac{\Omega R}{v} \tag{3}$$

Where Ω is the rotor angular speed [rad/s], R is the length of the blade [m] and v is the velocity of the wind [m/s].

This power coefficient can be obtained by analytical approximation. An approximated C_p curve is given by (Arifujjaman, Iqbal, & Quaocoe, 2009; González Acevedo, 2010; Rudion, Orths, & Styczynski, 2004; Tang, Guo, & Jiang, 2010):

$$C_p = 0{,}5176 \cdot \left(\frac{116}{\lambda_i} - 0{,}4 \cdot \beta - 5 \right) \cdot e^{\frac{-21}{\lambda_i}} + 0{,}0068 \cdot \lambda \qquad (4)$$

$$\lambda_i = \frac{1}{\frac{1}{\lambda + 0{,}08\beta} - \frac{0{,}035}{\beta^3 + 1}} \qquad (5)$$

C_p curves are shown for typical λ and β ranges in Figure 1 and Figure 2.

Figure 1: Power coefficient versus pitch angles and tip-speed-ratios
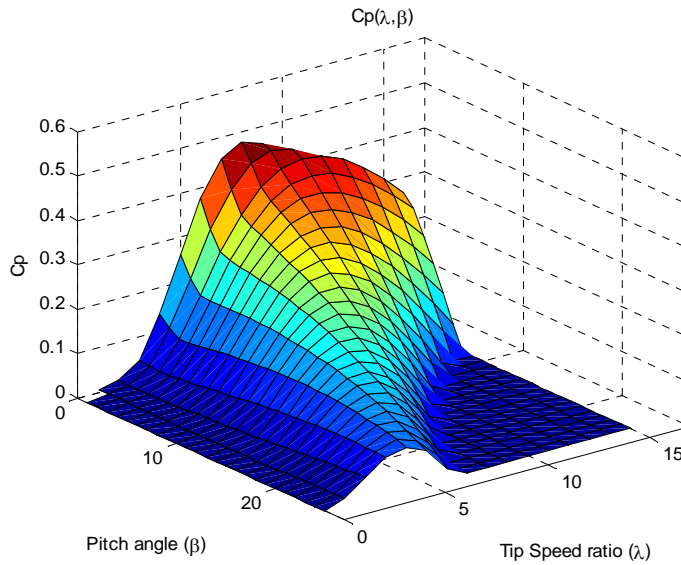
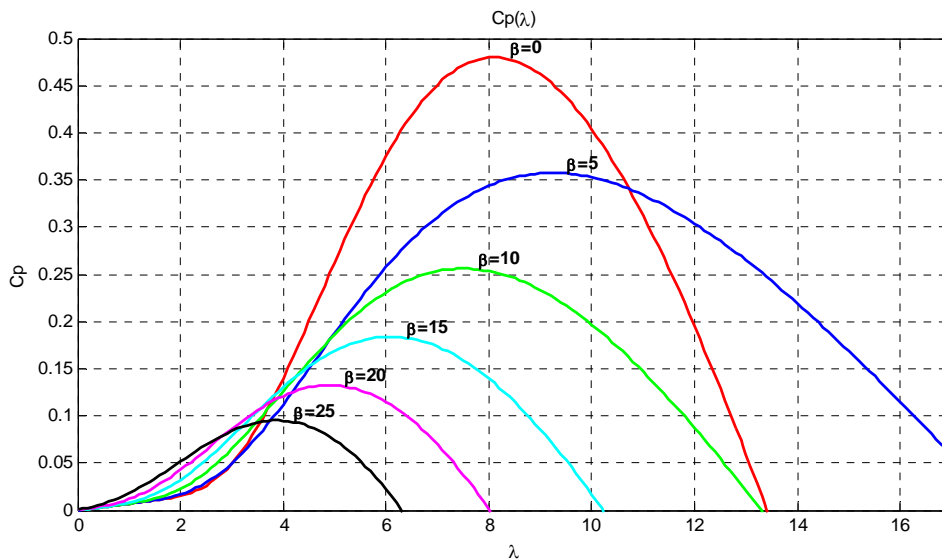**Figure 2: Power coefficient for different pitch angles**

Figure 2 illustrates that for β equal to zero, the C_p is maximum while increasing the pitch angle the power coefficient decreases. Taking this curve into account, Figure 3 depicts the pitch control strategy. Below rated wind speeds, the control goal is to maximize the amount of power produced, trying to keep the wind turbine operating as close as possible to its rated

power value. On the other hand, once the rated wind speed is reached, the pitch control acts over the blades rotating them so that the attack angle β from the wind is accordingly reduced in order to decrease the aerodynamic power. Thus, the blade pitch control assures the turbine shaft torque will remain within predefined limits.

Figure 3: Power at different wind speed
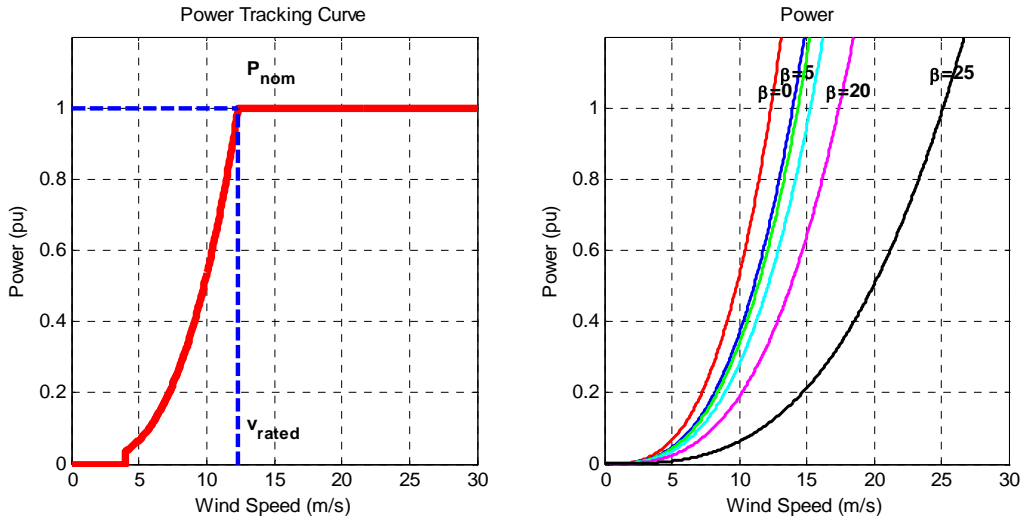
3. Analysis of the DFIG

Doubly-fed induction generators consist of a wound rotor induction generator with the stator windings connected directly to the grid and the rotor windings connected to it through a four-quadrant AC-DC-AC power converter, as Figure 4 shows. The DFIG allows an independent control of active and reactive power. The AC-DC-AC converter is divided in two components, the rotor side converter and the grid side converter. The capacitor between rotor and grid side converters behaves as a DC voltage source. The rotor side converter is used to control the wind turbine output power and the voltage measured at the grid terminals, while the grid side converter is used to regulate the voltage of the DC bus capacitor (Khemiri et al., 2012; Petersson, 2005).

Figure 4: DFIG connection scheme
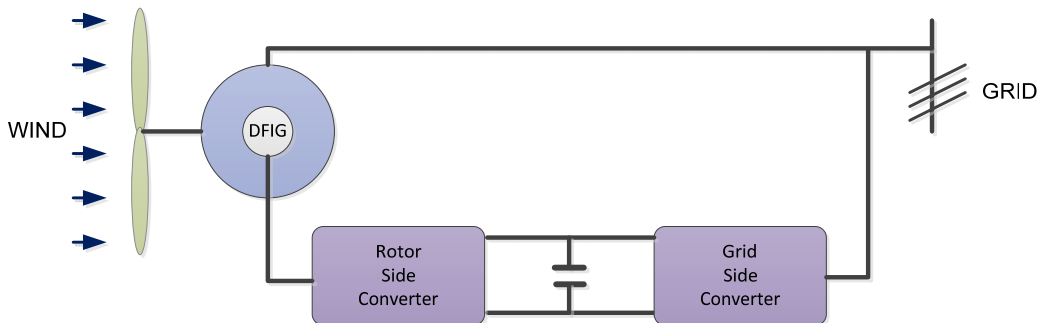
To simplify the analysis and control of three phase electrical machines, the dynamic equations in *abc*-frame are transformed into a new reference *dq0*-frame (Park transformation), which will be rotating at the synchronous angular speed of the system (García Franco, 2010; González Acevedo, 2010; Li, Haskew, & Jackson, 2008).

Accordingly, equations can be expressed from the stator and rotor voltages as:

$$V_{ds} = r_s \cdot i_{ds} + \frac{d}{dt} \cdot \lambda_{ds} - \omega_s \cdot \lambda_{qs} \tag{6}$$

$$V_{qs} = r_s \cdot i_{qs} + \frac{d}{dt} \cdot \lambda_{qs} + \omega_s \cdot \lambda_{ds} \tag{7}$$

$$V_{dr} = r_r \cdot i_{dr} + \frac{d}{dt}\lambda_{dr} - (\omega_s - \omega_r) \cdot \lambda_{qr} \tag{8}$$

$$V_{qr} = r_r \cdot i_{qr} + \frac{d}{dt}\lambda_{qr} + (\omega_s - \omega_r) \cdot \lambda_{dr} \tag{9}$$

The stator and rotor flux equations in the *dq0* reference frames are:

$$\lambda_{ds} = (L_{ls} + L_m) \cdot i_{ds} + L_m \cdot i_{dr} \tag{10}$$

$$\lambda_{qs} = (L_{ls} + L_m) \cdot i_{qs} + L_m \cdot i_{qr} \tag{11}$$

$$\lambda_{dr} = (L_{lr} + L_m) \cdot i_{dr} + L_m \cdot i_{ds} \tag{12}$$

$$\lambda_{qr} = (L_{lr} + L_m) \cdot i_{qr} + L_m \cdot i_{qs} \tag{13}$$

Where r_s, r_r, L_{ls} and L_{lr} are the resistances and leakage inductances of the stator and rotor windings; L_m is the mutual inductance and V_{ds}, V_{qs}, V_{dr}, V_{qr}, i_{ds}, i_{qs}, i_{dr}, i_{qr}, λ_{ds}, λ_{qs}, λ_{dr}, and λ_{qr} are the *d-* and *q-* components of the space vectors of stator and rotor voltages, currents, and fluxes; and ω_s and ω_r are the speeds of stator and rotor currents in electrical angles.

The equivalent circuits from the equations (6) to (13) are represented in Figure 5.

Figure 5: Electrical equivalent circuit in *dq* reference frame
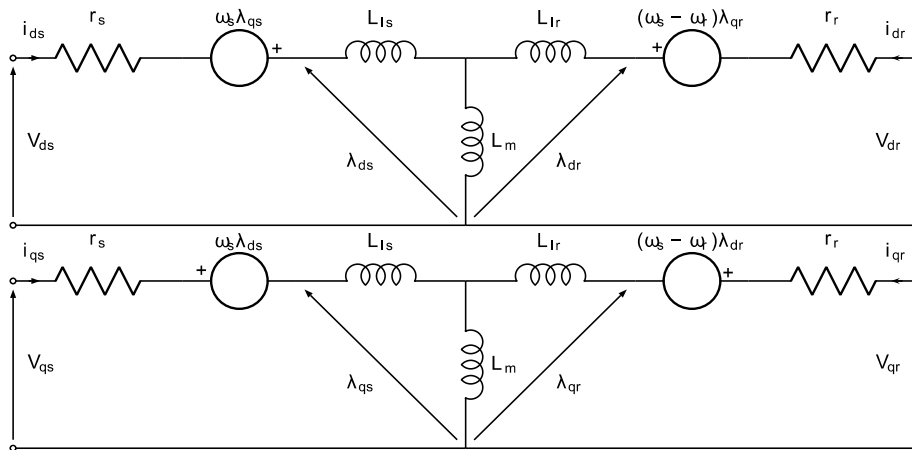
Finally, the electromagnetic torque created by the rotor windings can be expressed only in terms of flux linkages and currents in the *q*-axis and *d*-axis, defining p as the number of pole pairs and J as the inertia:

$$T_e = \frac{3}{2} \cdot p \cdot (\lambda_{ds} \cdot i_{qs} - \lambda_{qs} \cdot i_{ds}) \tag{14}$$

$$T_m - T_e = \frac{J}{p} \cdot \frac{d}{dt}\omega_r \tag{15}$$

3.1 Stator flux oriented reference frame

In order to achieve a separate control of active and reactive powers, stator flux oriented reference frame is used. The stator flux vector is aligned with the d-axis of the stator, the stator resistance is usually neglected and the frequency and amplitude of the stator or grid voltage is assumed to be constant (Arifujjaman et al., 2009; González Acevedo, 2010). Figure 6 depicts the phasor diagram where the alignment of the magnetic field vector and both *dq0-* and *abc-* reference frames can be seen (Faria, 2009).

Hence, if the *d*-axis of the reference frame is fully aligned with the stator magnetic field vector, these two expressions are easily obtained:

$$\lambda_{qs} = 0 \tag{16}$$

$$\lambda_{ds} = \lambda_{s\,total} \tag{17}$$

Combining equations (6) and (7) with (16) and (17) and considering the stator resistance r_s as zero, the following equations are obtained:

$$V_{qs} = \omega_s \cdot \lambda_{ds} = \omega_s \cdot \lambda_{s\,total} = constant \tag{18}$$

$$V_{ds} = 0 \tag{19}$$

Equations (18) and (19) show that the stator voltage is time-invariant and the voltage across the stator *d*-axis is negligible. The stator currents derive from the stator and rotor flux equations given in (10) and (11), taking into account that $\lambda_{qs} = 0$:

$$i_{qs} = \left(-\frac{L_m}{L_{ls}+L_m}\right) \cdot i_{qr} \tag{20}$$

$$i_{ds} = \left(\frac{\lambda_{ds}-L_m \cdot i_{dr}}{L_{ls}+L_m}\right) \tag{21}$$

Figure 6: Space vector diagram of stator fluxes in an induction machine
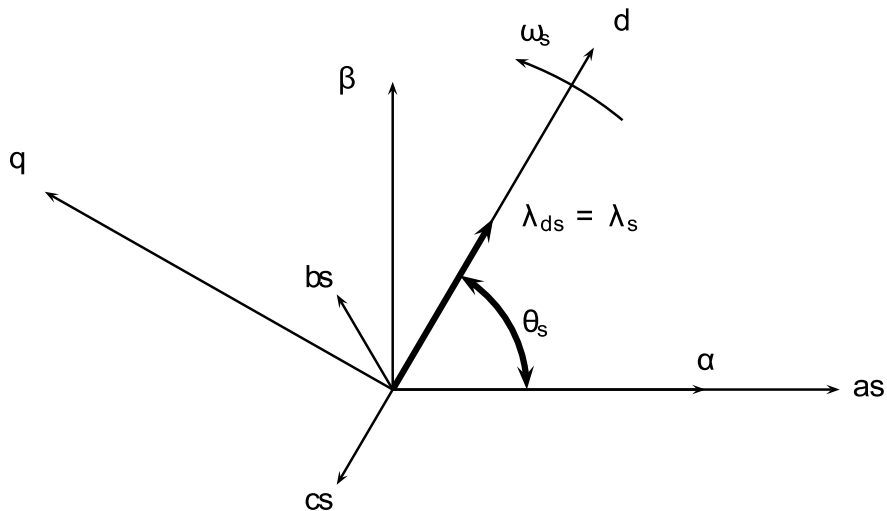
In equations (20) and (21), inductance and flux quantities are time-invariant. As a result, the stator *q*-axis and *d*-axis currents can be controlled by adjusting the rotor *d*-axis and *q*-axis currents, respectively.

The active and reactive powers in the stator windings are given by:

$$P_s = \frac{3}{2}\left(V_{ds} \cdot i_{ds} + V_{qs} \cdot i_{qs}\right) \tag{22}$$

$$Q_s = \frac{3}{2}\left(V_{qs} \cdot i_{ds} - V_{ds} \cdot i_{qs}\right) \tag{23}$$

These equations can be simplified by using equations (18) to (21) as follows:

$$P_s = \frac{3}{2}\left(V_{qs} \cdot i_{qs}\right) = -\frac{3}{2}\left(\frac{L_m}{L_{ls}+L_m}\right)\lambda_{ds}\omega_s i_{qr} \tag{24}$$

$$Q_s = \frac{3}{2}V_{qs}i_{ds} = \frac{3}{2}\left(\frac{\lambda_{ds}\omega_s}{L_{ls}+L_m}\right)(\lambda_{ds} - L_m i_{dr}) \tag{25}$$

The two equations above indicate that stator active and reactive power can be independently controlled by the rotor *d-* and *q-* axis currents respectively. Moreover, it can be seen that both the active and reactive powers are independent from the rotating speed (Dimopoulos et al., 2010; Kayıkc & Milanovic, 2007).

4. Power control method

Figure 7 displays the separated feedback control loops of *d-* and *q-* currents, that is, i_{dr} and i_{qr}. Controllers are tuned based on proportional plus integral (PI) design rules and algorithms. The reference current values $i_{dr_{ref}}$ and $i_{qr_{ref}}$ are calculated depending on the desired active and reactive power from (24) and (25). The control of the rotor currents in the *dq*-axis is being made indirectly through the rotor voltages V_{dr} and V_{qr}. In order to achieve the above, the correlation between the rotor voltages and the stator flux must be firstly determined (Pena, Clare, & Asher, 1996; Salman & Bradrzadeh, 2004).

Figure 7: Rotor side loop controller
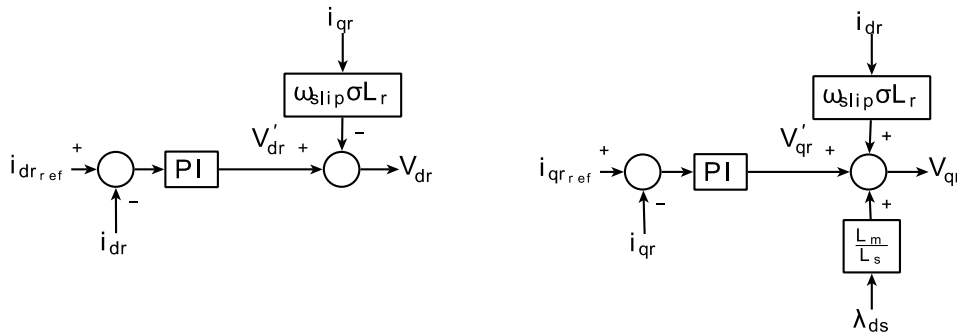
By substituting the stator currents (20) and (21) into the rotor fluxes equations (12) and (13) and being $L_r = L_{lr} + L_m$ and $L_s = L_{ls} + L_m$, one may get:

$$\lambda_{qr} = \sigma \cdot L_r \cdot i_{qr} \tag{26}$$

$$\lambda_{dr} = \sigma \cdot L_r \cdot i_{dr} + \frac{L_m}{L_s}\cdot\lambda_{ds} \tag{27}$$

$$\sigma = 1 - \frac{L_m^2}{L_s * L_r} \tag{28}$$

Where σ is defined as the total leakage factor.

Finally, the equations regarding the rotor voltage from (8) and (9) are generated as:

$$V_{dr} = r_r \cdot i_{dr} + \sigma \cdot L_r \cdot \frac{d}{dt} i_{dr} - (\omega_s - \omega_r) \cdot \sigma \cdot L_r \cdot i_{qr} \tag{29}$$

$$V_{qr} = r_r \cdot i_{qr} + \sigma \cdot L_r \cdot \frac{d}{dt} i_{qr} + (\omega_s - \omega_r)(\sigma \cdot L_r \cdot i_{dr} + \frac{L_m}{L_s} \cdot \lambda_{ds}) \tag{30}$$

It can be easily noticed that the control actions of the current closed loop to be computed by PI controllers see linear systems such as:

$$V_{dr}' = r_r \cdot i_{dr} + \sigma \cdot L_r \cdot \frac{d}{dt} i_{dr} \tag{31}$$

$$V_{qr}' = r_r \cdot i_{qr} + \sigma \cdot L_r \cdot \frac{d}{dt} i_{qr} \tag{32}$$

Then, actual control actions can be further computed from equations (29) and (30) as:

$$V_{dr} = V_{dr}' - \omega_{slip} \cdot \sigma \cdot L_r \cdot i_{qr} \tag{33}$$

$$V_{qr} = V_{qr}' + \omega_{slip}(\sigma \cdot L_r \cdot i_{dr} + \frac{L_m}{L_s} \cdot \lambda_{ds}) \tag{34}$$

where the coupling terms have been added. By transferring equations (31) and (32) into the Laplace domain, the transfer function of linear plant models can be generated and the PI controllers can be tuned according classical control design rules (Ogata, 2008).

5. Results

Figures 8 and 9 present some simulation results of the pitch control and power strategies implemented in the DFIG model. The aim of these conducted simulations was to demonstrate and verify the operation of the pitch control and the power control according to the criteria established in Figure 3. The variations of the wind speed are simulated as step responses with small random fluctuations.

Figure 8: Wind speed and pitch angle
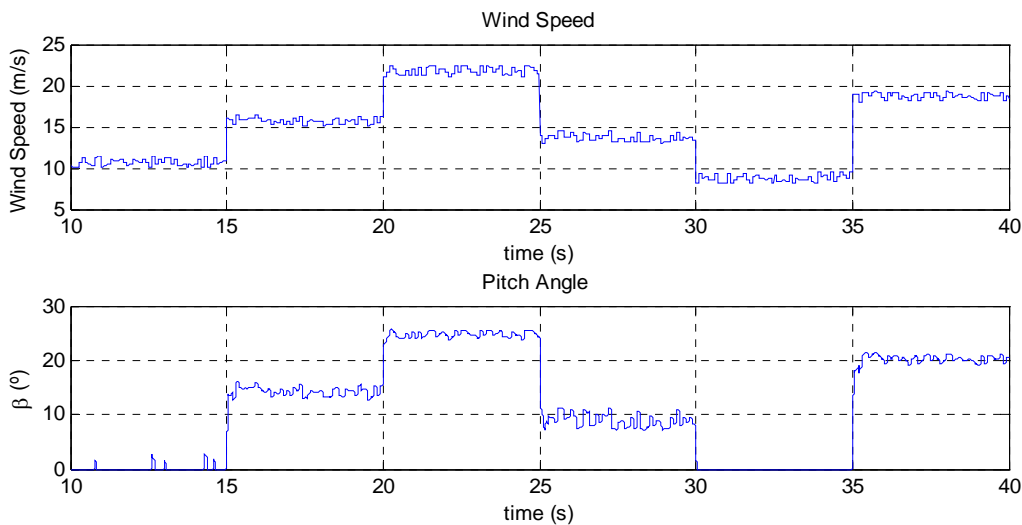
When wind speed increases to a value greater than the rated one, *β* also increases in order to keep the mechanical torque, and thus, the output power, equal to the rated one. Desired stationary operating points are obtained from maximum C_p values in Figure 2. In contrast, when the wind speed decreases below its nominal, *β* equals zero and power control acts trying to maximize the power extraction. Power control strategy was defined in Section 4, and later on, detailed simulations are included. According to all this, note in Figure 9 as the generated mechanical torque and power, in p.u. units, are in their nominal for wind speed over rated, and both ones decrease when the kinetic wind energy reduces.

**Figure 9: Mechanical torque and electrical power**
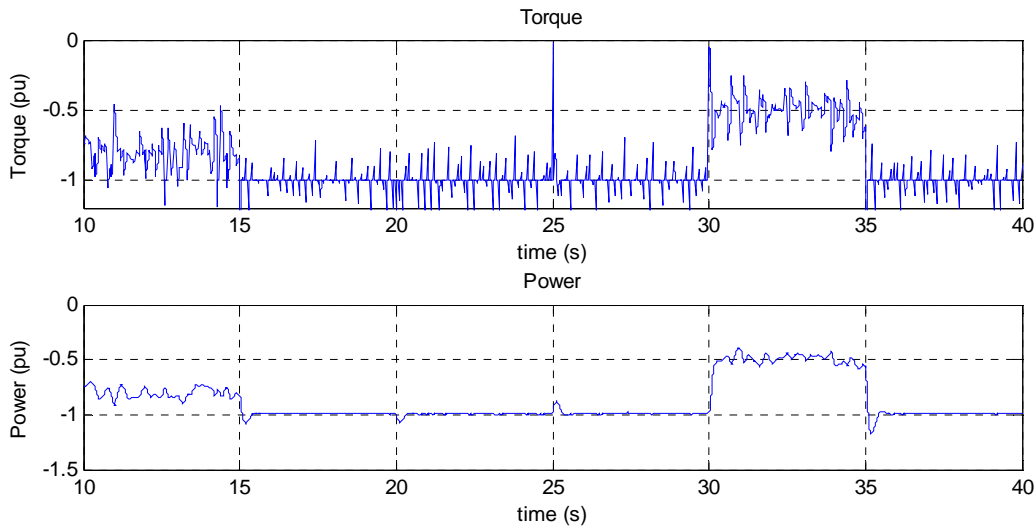
The Figures 10 and 11 show new detailed simulations of the power control. In this test case the desire for minimizing the stator windings reactive power $Q_s = 0$ has determined the reference value of the rotor direct axis $i_{dr,ref} = \frac{\lambda_{ds}}{L_m}$ with the help of equation (25). The respective reference value of the rotor quadrate axis, $i_{qr,ref}$, is calculated from (24) for a reference value of active power equal to $P_s = 2\ MW$. The PI controllers parameters are K_p=0.0064 and K_i=0.0582. These controllers were computed for linear plant models from (31) and (32) substituting DFIG parameters in Table 1 (Berrutti, 2010).

Table 1. DFIG Parameters

r_s	1.5e-3 Ω
r_r	2.0e-3 Ω
L_m	2.4e-3 H
L_s	2.5e-3 H
L_r	2.5e-3 H
J	70 kgm^2
p	2
V_{grid}	690V-50Hz

The Figure 10 and Figure 11 illustrate the response of the rotor currents (i_{dr}, i_{qr}) as well as the response of the active and reactive power (P_s, Q_s). Before instant t=5 sec, the rotor is short circuited. Then, PI controllers are applied at t=5 sec; when steady state is reached the active power takes its nominal and the reactive power is fully compensated. The green waveform corresponds to the reference value while the blue one represents the measured one.

Figure 10: Stator active (P_s) and reactive (Q_s) power
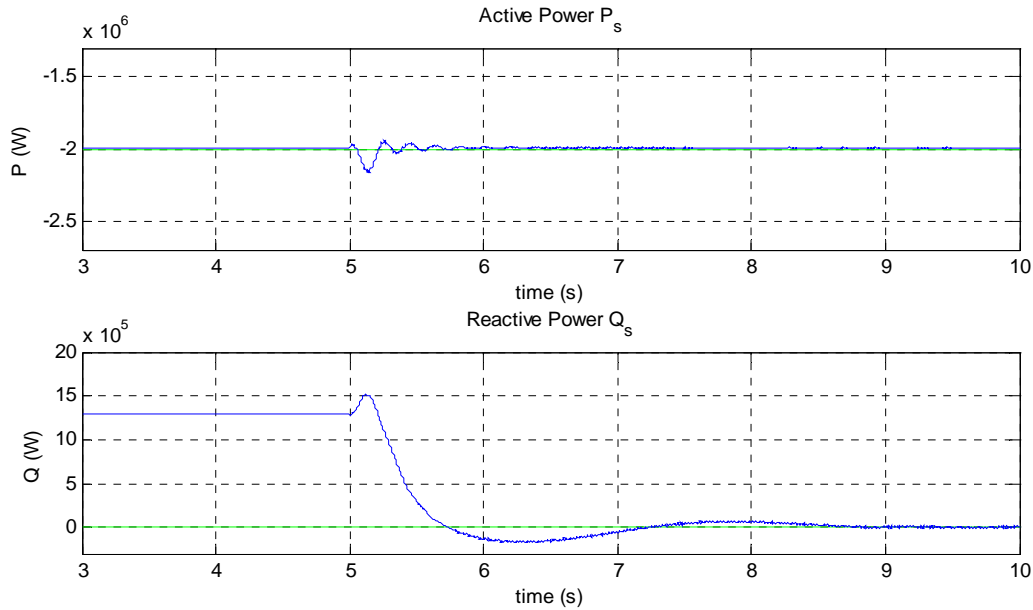
Figure 11: Rotor currents i_{dr} and i_{qr}
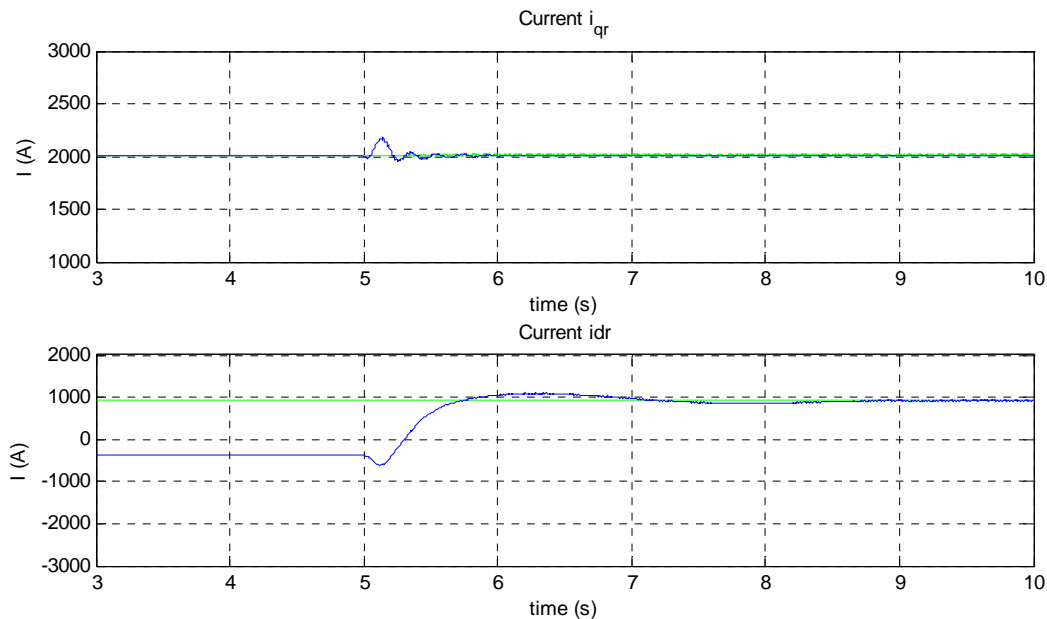
6. Conclusions

In this paper, a variable speed wind generator model based on a doubly-fed induction generator has been analysed. The modelling of the wind is presented and the effect of the pitch control over the wind turbine is analysed. For power control, the DFIG is examined and modelled in a rotating *dq*-reference frame. Then, the stator flux oriented vector control scheme is used, making possible to control the active power production by the generator through the *q*-axis rotor current while the reactive power is controlled by controlling the *d*-axis current. The graphic results prove that with the help of these controllers, the unity power factor between the DFIG stator windings and the grid can be achieved.

Acknowledgement

References

Arifujjaman, M., Iqbal, M. T., & Quaocoe, J. E. (2009). Vector Control of a DFIG Based Wind Turbine. *Journal of Electrical & Electronics Engineering*, 9(L), (1057–1066).

Berrutti, F. (2010). Control desacoplado de potencia activa y reactiva instantánea en aerogeneradores basados en máquinas de inducción doblemente alimentadas, 1–8.

Bujac, F., Stasiusk, P., & Valderrey, F. (2008). *Doubly Fed Induction Generator Fault Ride Though Control*.

Dimopoulos, E., Palomar Lozano, A., Ruiz De Vega, A., Suarez Gonzalez, A., Garcia Verde, L. F., Kyriakidis, I., & Hasmasan, A. (2010). *Analysis, modelling and control of a Doubly-Fed Induction Generator for Large Wind Turbines*. Aalborg University.

Faria, K. J. (2009). *Doubly-Fed Induction Generator based Wind Power Plant Models*. University of Texas, Austin.

García Franco, J. A. (2010). *Estudio de diferentes algoritmos de control en máquinas asíncronas doblemente alimentadas*. Universidad Politécnica de Cartagena.

González Acevedo, H. (2010). LQR controller design for a Variable Wind Speed Turbine - Diseño de un controlador LQR para una Turbina de Velocidad Variable. *Proceedings Of The 5th Conference Of The Euro-American Association On Telematics And Information Systems Eatis 2010, Universidad Tecnologica De Panama*, 1(1).

Kayıkc, M., & Milanovic, J. V. (2007). Reactive Power Control Strategies for DFIG Based Plants. *IEEE Transactions on energy conversion*, 22(2), 389–396.

Khemiri, N., Khedher, A., & Mimouni, M. F. (2012). Wind Energy Conversion System using DFIG Controlled by Backstepping and Sliding Mode Strategies. *International Journal of Renewable Energy Research*, 2(3), 421–434.

Li, S., Haskew, T. A., & Jackson, J. (2008). Power Generation Characteristic Study of Integrated DFIG and Its Frequency Converter. *Power and Energy Society General Meeting-Conversion and Delivery of Electrical Energy in the 21st Century*, 1–9.

Ogata, K. (2008). *Modern Control Engineering 5th Edition*. Pearson Educación.

Pena, R., Clare, J. C., & Asher, G. M. (1996). Doubly fed induction generator uising back-to-back PWM converters and its application to variable- speed wind-energy generation. *IEE Proc Electr. Power*, 143(3), 231–241.

Petersson, A. (2005). *Analysis , Modeling and Control of Doubly-Fed Induction Generators for Wind Turbines*.

Rudion, K., Orths, A., & Styczynski, Z. (2004). Modelling of variable speed wind turbines with pitch control. *2nd International Conference on Critical Infrastructures, Grenoble, France*, (October), 1–6.

Salman, S. K., & Bradrzadeh, B. (2004). New Approach for modelling Doubly Fed Induction Generator (DFIG) for grid-connection studies. *European wind energy conference an exibition, London*, (0), 1–13.

Tang, C. Y., Guo, Y., & Jiang, J. N. (2010). Nonlinear Dual-Mode Control of Variable- Speed Wind Turbines With Doubly Fed Induction Generators, 1–13.

Varela, J., & Valderrey, F. (2009). *A fast method to evaluate annual energy production of diffeerent off-shore wind farm configurations connected to a VSC-HVDC line transmission including evaluation of a new variable speed wind turbine concept based on RCC-WRIG*. Aalborg University.

Vázquez, F., González, M., Garrido, J., & Morilla, F. (2012). Control Multivariable: aplicación al control de un aerogenerador. *X Simposio CEA Ingeniería de Control*, 33–43.